Spectroscopy and electron detachment dynamics of C_4^-, C_6^-, and C_8^-

Yuexing Zhao, Esther de Beer,[a] Cangshan Xu, Travis Taylor, and Daniel M. Neumark
Department of Chemistry, University of California, Berkeley, California 94720, and Chemical Sciences, Division, Lawrence Berkeley National Laboratory, Berkeley, California 94720

Resonant multiphoton detachment spectroscopy has been used to obtain vibrationally resolved spectra of the $C\ ^2\Pi \leftarrow X\ ^2\Pi$ electronic transitions in C_4^-, C_6^-, and C_8^-. Transitions due to vibrational excitations in the totally symmetric stretching modes as well as the bending modes are observed. The electron detachment dynamics subsequent to multiphoton absorption are studied by measuring the electron emission time profiles and electron kinetic energy distributions. The observation of delayed electron emission combined with the form of the electron kinetic energy distributions indicates that these species undergo the cluster equivalent of thermionic emission. This interpretation is supported by comparing the experimental results to a microcanonical model for cluster thermionic emission. © *1996 American Institute of Physics.* [S0021-9606(96)01036-7]

I. INTRODUCTION

In this paper, we report the results of experimental studies of the spectroscopy and electron detachment dynamics of C_4^-, C_6^-, and C_8^-. The original motivation behind this work was to use resonant multiphoton detachment to map out electronic transitions in these anions, thereby complementing recent matrix isolation spectra obtained by Maier and co-workers.[1,2] In the course of these studies, it became apparent that the dynamics of electron detachment from the anions was at least as interesting as their spectroscopy. We find that electron detachment following multiphoton excitation is an indirect process, and in fact appears to proceed through the cluster analog of thermionic emission. This is a surprising result given the small number of atoms and relatively sparse electronic structure of these species, and therefore provides an interesting example of how an intrinsically macroscopic effect can manifest itself in a small molecule.

In contrast to neutral carbon clusters, the spectroscopy of carbon cluster anions is relatively unexplored. Anion photoelectron[3–5] spectroscopy, zero electron kinetic energy (ZEKE) spectroscopy,[6,7] and ion chromatography[8] all indicate that anions with less than ten atoms have linear ground states. The ZEKE spectra have yielded some anion vibrational frequencies (through hot bands) and spin–orbit splittings for the $^2\Pi$ ground states of C_5^- and C_6^-. Several experiments have identified excited electronic states of carbon cluster anions. The first such example was an excited state of C_6^- lying only 43 cm^{-1} below the detachment threshold; this was located by resonant two-photon detachment of C_6^-.[7] In a recent matrix absorption experiment, Maier and co-workers observed $C\ ^2\Pi \leftarrow X\ ^2\Pi$ electronic transitions for linear, mass-selected carbon cluster anions C_{2n}^- for $n=2$–10 (linear C_4^-, C_8^-, ... have $^2\Pi_g$ ground states, while C_6^-, C_{10}^-, ... have $^2\Pi_u$ ground states). These assignments are supported by *ab initio* calculations performed by Schmatz and Botschwina on the ground and excited states of C_4^-,[9] C_6^-,[10] and C_8^-.[11] An

excited state of C_5^- has recently been observed in the gas phase through resonant two-photon detachment.[12]

The matrix experiments suggest that the electronic spectroscopy of the C_{2n}^- anions can be studied in the gas phase using resonant two- or multiphoton detachment in which the first photon excites the $C\ ^2\Pi \leftarrow X\ ^2\Pi$ transition. We have recently carried out such a study of the $C\ ^2\Pi_u \leftarrow X\ ^2\Pi_g$ transition in C_4^-,[13] achieving rotational resolution for two of the vibrational bands. In this paper, vibrationally resolved resonant multiphoton detachment spectra of C_6^- and C_8^- are presented and compared with the matrix spectra. In addition, the electron detachment dynamics of the three anions are studied by measuring the photoelectron spectra and electron emission rate that result from resonant multiphoton detachment through various excited electronic and vibrational levels. A comparison of these measurements to previous investigations of a variety of clusters suggests that the three carbon cluster anions investigated here undergo thermionic emission subsequent to resonant multiphoton absorption.

Thermionic emission from macroscopic surfaces can be described as direct ejection of electrons from a hot surface as the result of heating to the point where electron energies exceed the work function of the surface. The temperature dependence of the electron emission rate from hot surfaces is well described by the Richardson–Dushman equation.[14] The analogous process can occur in finite-sized clusters if, subsequent to excitation of the cluster by whatever means, randomization of the excitation energy amongst the various electronic and vibrational degrees of freedom in the cluster occurs on a time scale faster than electron detachment. Under these circumstances, the electron ejection dynamics can be considered as an activated statistical process in which the emission rate is determined solely by the total energy (or temperature) of the cluster.[15]

One signature of thermionic emission in a cluster is the observation of delayed electron emission, that is, electron emission occurring as long as several microseconds after the excitation process. Delayed electron emission has been observed following multiphoton excitation of small neutral metal clusters[16–18] and in a series of experiments on C_{60} and

several of the larger fullerenes.[19–24] It has been observed in $Si_n^\pm$ and C_{60}^- subsequent to hyperthermal collisions of these clusters[25] with a surface, and in C_{60}^- formed in "hot" ion sources.[26,27] The emission rates can be reproduced with at least qualitative accuracy by relatively straightforward statistical models; the expression derived by Klots[15] for the emission rate as a function of cluster "temperature" has proved particularly useful in this regard. Based on this, the above experiments are now considered to be examples of thermionic emission in clusters, although there has been some discussion about whether or not this is the correct mechanism in the C_{60} experiments.[28,29]

The photoelectron spectrum of a neutral or anion cluster provides a second means to test for thermionic emission. In direct ionization (detachment), the photoelectron spectrum reflects the allowed electronic transitions and Franck–Condon factors between the neutral (anion) and positive ion (neutral). For thermionic emission from a bulk material, on the other hand, the electron kinetic energy distribution is essentially thermal, reflecting the temperature of the material, and similar results are expected for a finite cluster. Thus an electron kinetic energy distribution dominated by low-energy electrons is a possible signature of thermionic emission from a cluster. Such effects have been seen in the multiphoton ionization of C_{60},[23] the single-photon detachment of C_{60}^-,[30] and, perhaps most convincingly, in the one-photon detachment of W_n^- ($n=3–10$) anions.[31]

The three carbon cluster anions considered in this work, C_4^-, C_6^-, and C_8^-, are smaller and much less electronically complex species than the metal clusters and fullerenes discussed above. Nonetheless, we find that the photoelectron spectra of C_4^- and C_6^- resulting from multiphoton detachment are indeed peaked near zero kinetic energy, in marked contrast to the one-photon photoelectron spectra of these anions.[4] We also observe delayed electron emission from C_6^- and C_8^- following resonant multiphoton absorption at selected photon energies. Considerable care is taken to determine the number of absorbed photons responsible for the delayed emission at each photon energy. One can then determine the electron emission rate constants as a function of total energy. These can be directly compared with calculated rate constants for thermionic emission using the *microcanonical* expressions developed by Klots.[15] The resulting good agreement indicates that we are indeed observing the analog of thermionic emission from these very small clusters.

II. EXPERIMENT

For each negative ion, three types of measurements were performed: (1) wavelength scans, in which the resonant multiphoton detachment spectra of C_4^-, C_6^-, and C_8^- were obtained, (2) measurements of the electron emission time profiles subsequent to photodetachment with one or two laser pulses, and (3) photoelectron spectroscopy of C_4^- and C_6^- following multiphoton excitation. Experiments (1) and (2)

were done on a pulsed tunable laser photodetachment apparatus,[7,32] while experiment (3) was performed on a time-of-flight photoelectron spectrometer.[33]

The same ion source is used in all three experiments. Carbon cluster anions are generated in a pulsed discharge source which has been described previously.[34] Briefly, a gas mix of 3% acetylene, 1% CO_2 in Ne is pulsed from a piezoelectric valve and passes through the discharge region in which a pulsed field is applied just after the valve opens. The resulting mixture of ions and neutrals passes through a short clustering channel (5 mm long, 2.5 mm i.d.) prior to expansion into the source vacuum chamber. To improve stability of the ion signal, a 1 keV electron beam intersects the expanding molecular beam. The pulsed beam then passes through a 2 mm diameter skimmer 1.5 cm from the discharge assembly and into the next vacuum region. We found that the distance between the pulsed valve and the skimmer strongly affects the temperature of the negative ions, with the temperature dropping as this distance is increased.

In experiments (1) and (2), negative ions that pass through the skimmer are collinearly accelerated to 1 keV. Ions are separated according to their mass-to-charge ratios in a 2 m coaxial beam-modulated time-of-flight mass spectrometer.[35] The mass-selected ion packet is crossed by the laser beams, and all the electrons generated via photodetachment are extracted perpendicularly by a weak electric field and collected by a 40 mm diameter multichannel plate (MCP) detector. The ion signal is monitored by another MCP detector that lies along the ion beam axis about 20 cm downstream from the laser interaction region. The electron signal is normalized to the ion signal and laser power.

The one-color resonant multiphoton detachment spectra in experiment (1) are obtained by measuring the electron signal intensity while scanning the laser wavelength of a dye laser pumped with a XeCl excimer laser. Electron signal intensity is measured using a gated detection scheme, in which electron signal appearing inside of a 60 ns wide gate is integrated and converted into digital signal using a CAMAC analog-to-digital converter. Each spectrum is the result of signal averaging over 500 laser shots/point. The measured bandwidth of the laser beam is ca. 0.3 cm^{-1}. The laser is calibrated by measuring the absorption spectra of an iodine cell or a Fe–neon cathode lamp. The laser fluence used in this type of experiment is typically in the range of 30–60 mJ/cm^2. The laser pulse width is approximately 30 ns FWHM. To obtain the wavelength scans reported here, the following laser dyes were used: Oxazine 750, Pyridine I, DCM, Rhodamine 640, Rhodamine 610, Rhodamine 590, Coumarin 540, Coumarin 503, Coumarin 480, Coumarin 460, Coumarin 440, Exalite 416, and DPS.

Two-color multiphoton detachment spectra were obtained for C_6^-. In these experiments, a weak laser pulse (ca. 2 mJ/cm^2) excites the bound-bound electronic transition, and a stronger pulse (ca. 40 mJ/cm^2) selectively detaches the electronically excited ions. As discussed in our study on C_4^-,[13] this considerably reduces saturation of the bound-bound transition compared to the one-color experiment, in which a strong pulse must be used to see sufficient detachment sig-

nal. In the two-color experiment, the excitation pulse comes from the excimer-pumped dye laser, while the detachment pulse comes from a YAG-pumped dye laser. The detachment laser wavelength is fixed at 635.5 nm which is non-resonant with any transition.

In experiment (2), electron emission time profiles are recorded at various fixed photon energies. This is achieved by collecting all the electron signal subsequent to the laser pulse(s) with a 500 MHz digitizing oscilloscope, typically signal averaging over 10^4 laser shots. The electrons emitted after the ion packet has passed through the electron detector region cannot be collected, restricting the experiment to time delays less than ca. 700 ns after the laser pulses. Both one and two-color experiments were performed, using the same laser arrangements as for experiment (1). As will be discussed below, the two-color experiments are needed in order to determine the total number of photons absorbed. In these experiments, it is important to distinguish between electrons produced by the two lasers, so the detachment pulse is typically fired 200 ns after the excitation pulse. The detachment pulse crosses the ion beam several mm downstream of the excitation pulse (9 mm for C_6^- at 1 keV, for example) to insure that the two pulses interact with the same ions.

Electron kinetic energy distributions, i.e., experiments of type (3), are measured in an anion time-of-flight photoelectron spectrometer which has been described in detail elsewhere,[33] although a reflectron stage has recently been added for improved mass resolution.[36] Ions are produced in the same manner described above. Anions generated from the discharge source pass through a skimmer and are perpendicularly extracted with a pulsed electric field into a time-of-flight mass spectrometer. Ions of the desired mass are selectively detached by a properly timed pulse of light from the excimer-pumped dye laser or one of the harmonics of a YAG laser. After photodetachment, a dual microchannel plate detector at the end of a 1 m field-free flight tube detects a small fraction of the photoelectrons. The electron flight times are measured, and from this the electron kinetic energies (eKE) are obtained; the instrumental resolution is 8 meV at 0.65 eV and degrades as $(eKE)^{3/2}$ at higher electron kinetic energy. The detection efficiency of the time-of-flight analyzer is relatively constant for electrons with >0.2 eV kinetic energy, and below this the detection efficiency drops considerably.

III. RESULTS

A. Resonant multiphoton detachment spectra of C_4^-, C_6^-, and C_8^-

The one-color resonant multiphoton detachment spectra of C_4^-, C_6^-, C_8^- are shown in Fig. 1. The spectra become more complex as the number of carbon atoms increases. The C_4^- spectrum has been discussed in detail elsewhere;[13] it is included here for comparison.

The C_6^- spectrum was recorded from 15 000–23 000 cm^{-1}. The region of this spectrum from 16 200–19 200 cm^{-1} is shown in more detail in Fig. 2. The most intense peak occurs at 16 476 cm^{-1} and appears to be the origin of an electronic transition. Several very weak transitions, pre-
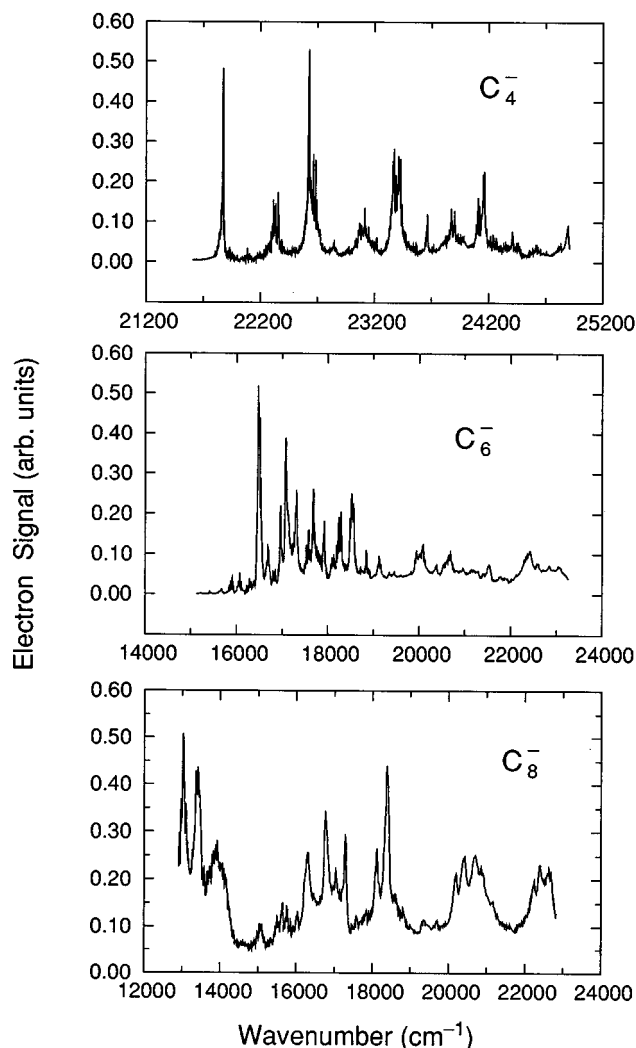

FIG. 1. One-color resonant multiphoton detachment spectra of C_4^-, C_6^-, and C_8^-.
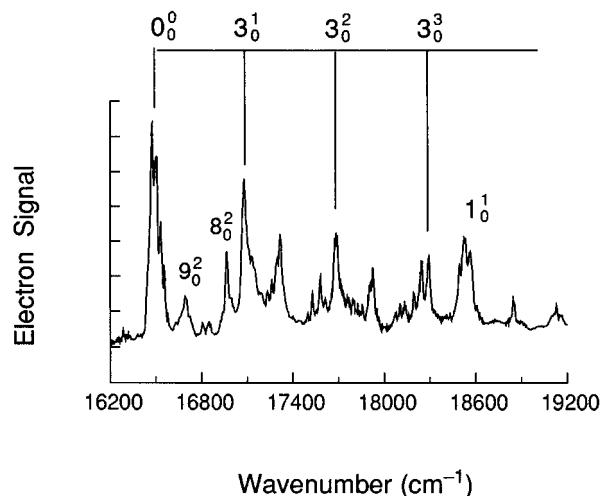

FIG. 2. Expanded C_6^- spectrum and vibrational assignments.

TABLE I. Peak positions, relative energies, assignments, and vibrational frequencies from one-color multiphoton detachment spectrum of C_6^-.

Peak position (cm^{-1})	Relative energies (cm^{-1})	Assignment	Frequencies (cm^{-1})	
			Expt.	Calculated[a]
15 912	−564	3_1^0	$\sigma_g''564$	637
16 075	−401	8_2^0	$\pi_g''201$	
16 476	0	Origin		
16 696	220	9_0^2	$\pi_u 110$	
16 965	489	8_0^2	$\pi_g 245$	
17 078	602	3_0^1	$\sigma_g 602$	600
17 316	840	$3_0^1 9_0^2$		
17 685	1209	3_0^2		
17 929	1453	$3_0^2 9_0^2$		
18 243	1767	2_0^1	$\sigma_g 1767$	1805
18 294	1818	3_0^3		
18 528	2052	1_0^1	$\sigma_g 2052$	2189
18 845	2369			
19 129	2653	$1_0^1 3_0^1$		
19 940	3464	2_0^2		
20 088	3612			
20 697	4221			
22 428	5952			

[a]From Ref. 10 (harmonic frequencies).

TABLE II. Peak positions, relative energies, assignments, and vibrational frequencies from one-color multiphoton detachment spectrum of C_8^-.

Peak position (cm^{-1})	Relative energies (cm^{-1})	Assignment	Frequencies (cm^{-1})
12 921	−42		
12 963	0	Origin	
13 023	60		
13 096	133		
13 362	399		
13 416	453	4_0^1	$\sigma_g 453$
13 920	957	4_0^2	
15 050	2087	1_0^1	$\sigma_g 2087$
15 646	2683		
16 305	3342	Origin	
16 766	3803		
17 292	4329		
18 125	5162		
18 392	5429		
20 202	7239		
20 408	7445		
20 702	7739		
22 400	9437		

sumably hot bands from vibrationally excited anions, are observed to the red of the origin. To the blue of the origin, the most prominent feature is a progression with a spacing of ca. 600 cm^{-1}. Many other features are also observed. Figure 2 shows that the origin peak actually consists of 3–4 partially resolved peaks which are separated from each other by ca. 25 cm^{-1}. The narrowest peaks in the spectrum, typically 10–15 cm^{-1} at FWHM, are significantly broader than the laser bandwidth. Peaks are generally broader at the blue end of the spectrum. Peak positions and vibrational assignments (see below) are listed in Table I.

The C_6^- spectrum from 16 978–17 123 cm^{-1} obtained from a two-color scan is shown in Fig. 3. Compared to the
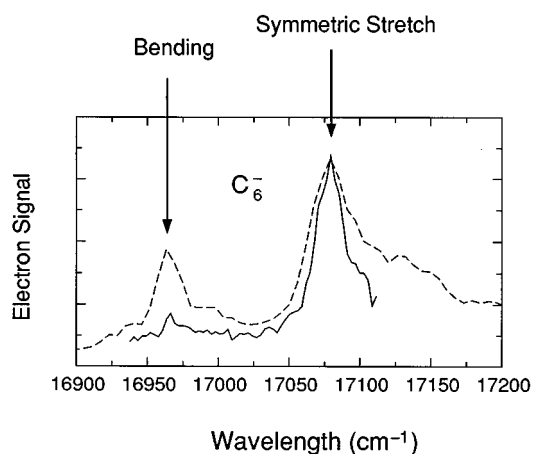

FIG. 3. Two-color and one-color resonant multiphoton detachment spectra of C_6^-. Solid line: two-color spectrum, laser wavelength of the excitation laser is scanned while the detachment laser is fixed at 15 740 cm^{-1}; the detachment laser fluence is 2 mJ/cm^2. Dashed line: one-color spectrum, laser fluence is 30 mJ/cm^2.

one-color scan (dashed line), the peak at 17 078 cm^{-1} is noticeably narrower and the peak at 16 696 cm^{-1} is less intense by about a factor of 5. We associate both of these effects with less saturation in the two-color spectrum due to lower fluence of the excitation laser.

The C_8^- multiphoton detachment spectrum from 12 950–23 000 cm^{-1} is shown at the bottom of Fig. 1. No peaks were observed to the red of the large peak at 12 963 cm^{-1}, and this appears to be the origin of an electronic transition. The origin and the two peaks to the blue of the origin are spaced by ca. 450 cm^{-1}; this presumably represents a vibrational progression. Further to the blue, the spectrum is quite complex and irregular; it is likely that multiple electronic transitions are contributing to the spectrum in this region. Also, the baseline of the spectrum is above zero all the way across the photon energy region shown. Peak positions and assignments (see below) are given in Table II.

B. Electron emission time profiles

At all photon energies, the electron emission time profiles of C_4^- following multiphoton excitation are prompt. The time profile of the electron signal is identical to the laser pulse time profile, which is ca. 30 ns wide, and no delayed emission is observed.

The situation is different for C_6^- and C_8^-. The electron emission time profiles of C_6^- measured at various photon energies are shown in Fig. 4. At 17 683 cm^{-1}, and all lower energies, the electron signal is prompt. However, delayed electron emission appearing long after the laser pulse is observed at higher photon energies. For example, at 19 944 cm^{-1}, both delayed electrons and prompt electrons are seen; the abrupt decrease of the delayed electron signal beyond 550 ns is due to anions flying out of the electron detector region. At 20 695 cm^{-1}, the delayed electron emission decays more quickly. By 22 411 cm^{-1}, the decay of the de-
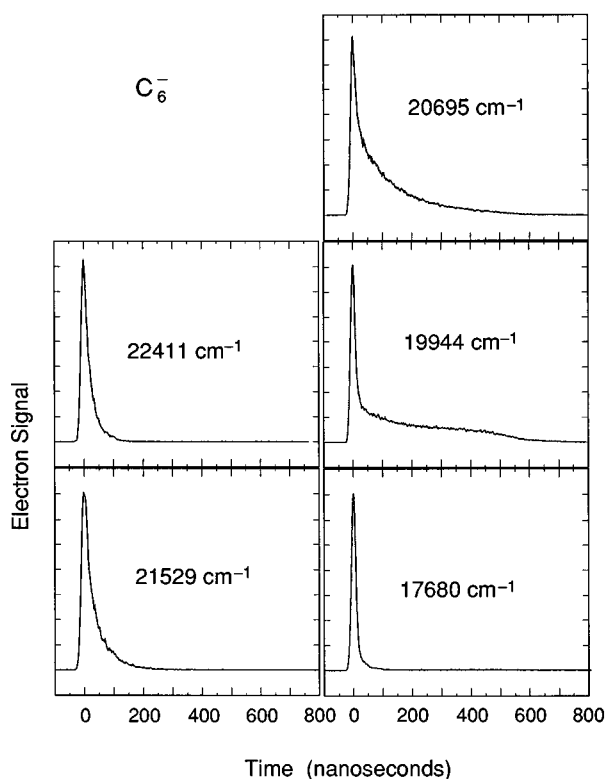
FIG. 4. Electron emission time profiles from resonant multiphoton detachment of C$_6^-$ at various photon energies. The time width at FWHM of the laser pulse is 30 ns.
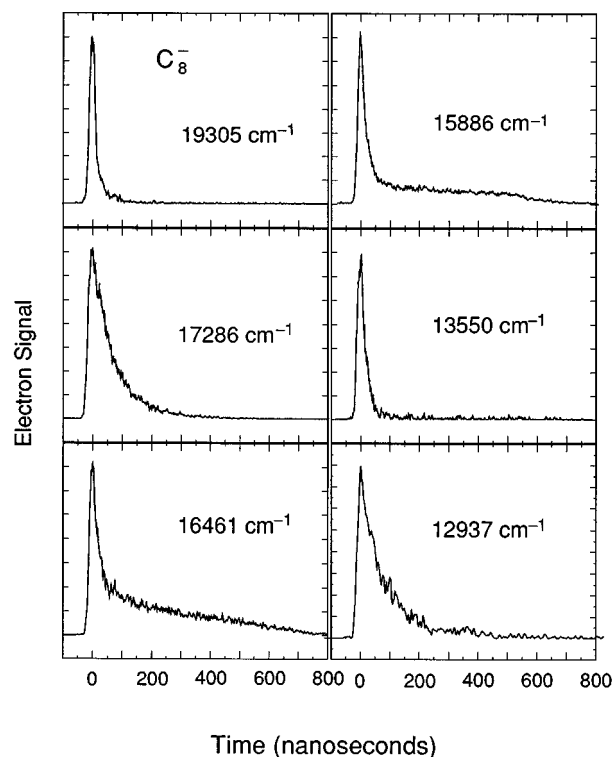

FIG. 5. Electron emission time profiles from resonant multiphoton detachment of C$_8^-$ at various photon energies. The time width at FWHM of the laser pulse is 30 ns.

layed emission is sufficiently fast to be indistinguishable from prompt emission. The delayed electron signal decays exponentially with time. Rate constants can be obtained by fitting the decays with a first-order rate constant. The electron emission rate constants at the various photon energies are shown in Table III.

For C$_6^-$, once delayed electron emission appears, its rate monotonically increases with increasing photon energy. However, the situation with C$_8^-$ multiphoton detachment is more complicated. Figure 5 shows electron signal time pro-

files of C$_8^-$ at various photon energies. At 12 937 cm^{-1}, the band origin, delayed electron signal is observed, and by 13 550 cm^{-1}, the delayed electron emission rate is almost as fast as prompt electrons. However, delayed electron emission reappears at 15.886 cm^{-1} and again gradually becomes faster as the photon energy is further increased. The electron emission rates vs. photon energies are shown in Table IV.

To further characterize delayed electron emission, two additional experiments were performed: (1) laser power de-

TABLE III. Thermionic emission rate constants for C$_6^-$ at various photon energies.

Photon energy (cm^{-1})	Number of photons[a]	Total photon energy (cm^{-1})	Rate constant (s^{-1})
19 128	2	38 256	$1.00(40)\times10^6$
19 946	2	39 892	$2.42(20)\times10^6$
20 073	2	40 145	$2.86(16)\times10^6$
20 359	2	40 717	$4.70(15)\times10^6$
20 459	2	40 917	$6.10(15)\times10^6$
20 526	2	41 051	$5.90(15)\times10^6$
20 696	2	41 391	$7.60(15)\times10^6$
20 965	2	41 929	$1.06(3)\times10^7$
21 044	2	42 088	$1.30(4)\times10^7$
21 151	2	42 301	$1.38(4)\times10^7$
21 529	2	43 057	$1.92(7)\times10^7$
21 882	2	43 764	$2.60(27)\times10^7$
22 414	2	44 828	$3.70(40)\times10^7$

[a]See Sec. IV B 2.

TABLE IV. Thermionic emission rate constants for C$_8^-$ at various photon energies.

| Photon energy (cm^{-1})	Number of photons[a]	Total photon energy (cm^{-1})	Rate constant (s^{-1})
16 057	3	48 170	$1.40(30)\times10^6$
16 116	3	48 348	$1.50(30)\times10^6$
16 134	3	48 403	$1.70(30)\times10^6$
16 461	3	49 383	$2.50(20)\times10^6$
16 543	3	49 628	$2.90(20)\times10^6$
16 625	3	49 875	$3.50(20)\times10^6$
16 722	3	50 167	$4.10(20)\times10^6$
16 764	3	50 293	$4.50(20)\times10^6$
17 036	3	51 107	$7.70(30)\times10^6$
17 182	3	51 546	$1.08(6)\times10^7$
17 286	3	51 858	$1.23(7)\times10^7$
17 376	3	52 129	$1.63(14)\times10^7$
12 937	4	51 746	$1.18(10)\times10^7$
13 021	4	52 083	$1.45(12)\times10^7$

[a]See Sec. IV B 3.
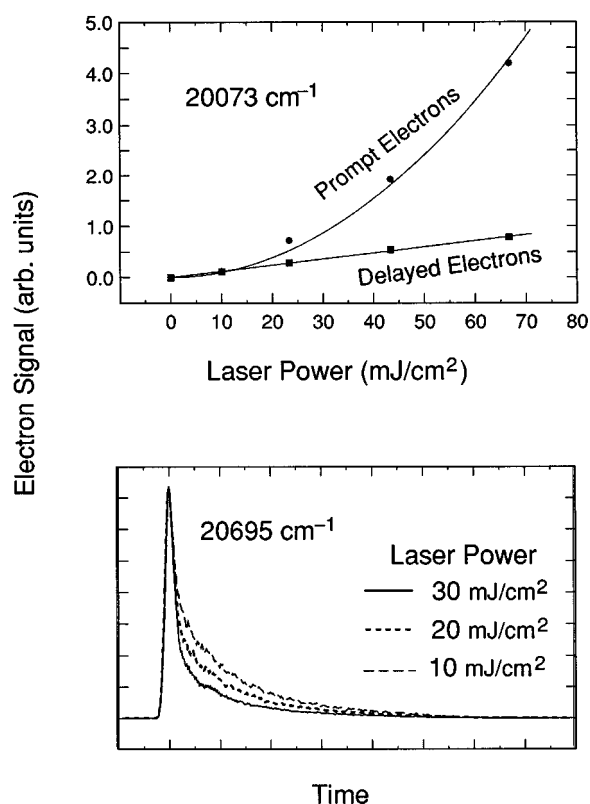
FIG. 6. Laser fluence dependence for the prompt and delayed electron signal of C_6^- multiphoton detachment at two photon energies where both type of emission are observed. Top figure shows integrated prompt and delayed signal as function of laser fluence. Bottom figure shows entire emission profiles at three laser fluences.

FIG. 7. Two-color measurements of electron emission from C_6^- multiphoton detachment. (top) Solid trace is the electron signal time profile after C_6^- interacts with two separated laser pulses: (1) at 17 077 cm^{-1} and (2) at 22 873 cm^{-1}; dashed trace is the electron signal time profile when the first laser pulse is blocked. (bottom) Two-color electron signal time profile (solid line) is compared to one-color electron emission (dashed line) at (3) 19 975 cm^{-1}. Intensity is normalized to show the almost identical delayed electron emission traces from these two different experiments. Note that $2h\nu_3 = h\nu_1 + h\nu_2$.

pendence studies of delayed electron emission and prompt electron emission and (2) two-color measurements of the time profiles for delayed electron emission.

Figure 6 shows the laser power dependence of the delayed electron signal and the prompt electron signal in C_6^- multiphoton detachment. At 20 073 cm^{-1}, as shown in the top half of Fig. 6, the delayed electron signal is linearly proportional to laser fluence, while the prompt electron signal has a quadratic dependence on the laser fluence. This is shown in a different fashion in the bottom half of Fig. 6, where the time profiles at 20 695 cm^{-1} at three different laser fluences are superimposed, normalized to the maximum at 0 ns. The relative intensity of the delayed vs prompt electron signal increases when laser fluence decreases, which again indicates that the prompt electron signal has a steeper laser fluence dependence than the delayed electron signal.

The results of the two-color experiment are shown in Fig. 7. In the top half of this figure, the solid trace shows the electron signal time profile resulting from two laser pulses separated temporally by ca. 200 ns and spatially by ca. 9 mm. The photon energies for the first and second laser pulses are $h\nu_1 = 2.12$ eV (17 077 cm^{-1}) and $h\nu_2 = 2.84$ eV (22 873 cm^{-1}), respectively. The first peak centered at 0 ns is the detachment signal from $h\nu_1$ alone; only prompt emission is observed. The second peak beginning at 200 ns shows both
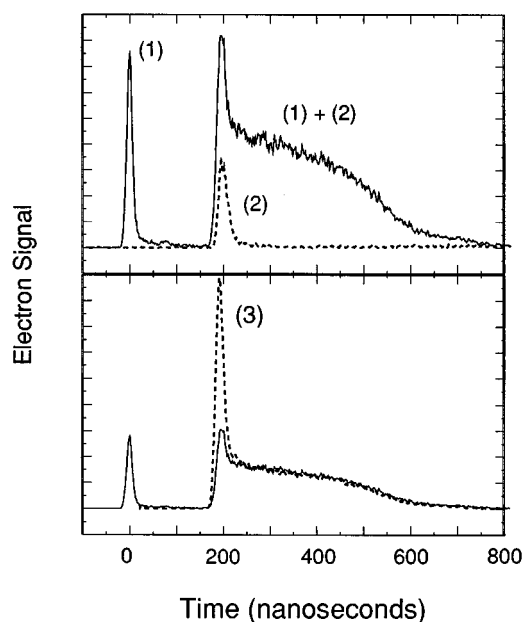
prompt and delayed emission. The dashed trace shows the electron signal when the first laser pulse is blocked, i.e., the signal due to multiphoton detachment by the second laser alone; only prompt emission is seen. Hence, *the ions must absorb at least one photon from each laser pulse for delayed emission to occur.*

In the bottom half of Fig. 7, the two-color electron signal time profile (solid trace) is compared to the one-color electron signal time profile at $h\nu_3 = 2.48$ eV (19 969 cm^{-1}). This photon energy was chosen so that $2h\nu_3 = h\nu_1 + h\nu_2$. The two traces show the same delayed electron emission rate. The significance of the results in Fig. 7 will be discussed in Sec. IV.

C. Single photon and multiphoton photoelectron spectra of C_4^- and C_6^-

The top halves of Figs. 8 and 9 show single-photon photoelectron spectra of C_4^- and C_6^-, respectively, at photon energy $h\nu = 4.66$ eV. The photoelectron spectra resulting from resonant multiphoton detachment of the two anions are shown in the bottom halves of Figs. 8 and 9; in both spectra, the laser photon energy is resonant with the corresponding origin transition of the $C\ ^2\Pi \leftarrow X\ ^2\Pi$ electronic band in Fig. 1. Clearly, the single-photon and multiphoton photoelectron spectra are completely different.

The single-photon spectra are highly structured. In both of these spectra, the photon energy exceeds the electron af-
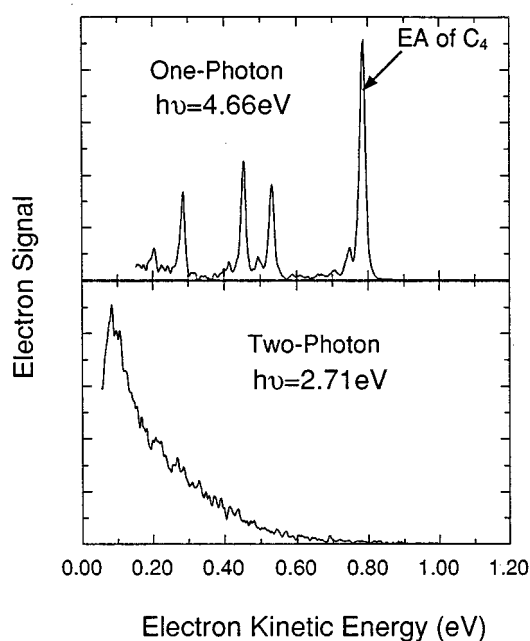
FIG. 8. Time-of-flight photoelectron spectra of C_4^-. (Top) One-photon direct detachment with photon energy of 4.66 eV; (bottom) resonant multiphoton detachment with photon energy of 2.71 eV. The electron affinity of linear C_4 is 3.88 eV.
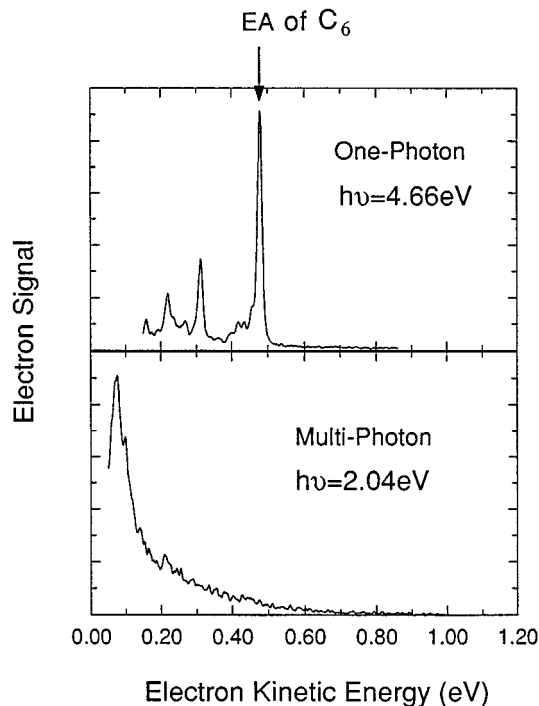

FIG. 9. Time-of-flight photoelectron spectra of C_6^-. (top) One-photon direct detachment with photon energy 4.66 eV; (bottom) resonant multiphoton detachment with photon energy 2.04 eV. The electron affinity of linear C_6 is 4.18 eV.

finity of the neutral carbon cluster, 3.88 eV for C_4 and 4.18 eV for C_6,[4] so direct detachment to the neutral $+ e^-$ continuum occurs. These spectra represent improvements on earlier work in our laboratory[4] and will be discussed in more detail in a future publication.[36] For current purposes, it suffices to note that the sharp structure in these spectra corresponds to transitions between the anion and various electronic and vibrational levels of the neutral species.

In contrast, the multiphoton photoelectron spectra peak at low eKE ($\sim$0.1 eV) and decrease continuously towards higher eKE, with no evidence of any vibrational structure. The C_4^- and C_6^- spectra are similar except that the decay towards higher eKE is more rapid in the C_6^- spectrum. As mentioned in the previous section, the transmission efficiency of the electron time-of-flight analyzer decreases for electrons with eKE below 0.2 eV, so the observed maximum might be due to this instrumental cut-off for slow electrons. Note that multiphoton photoelectron spectra were not taken for C_8^- because delayed emission occurs at the origin of the $C \, ^2\Pi \leftarrow X \, ^2\Pi$ transition (see Fig. 5); under such circumstances, one cannot use time-of-flight for electron energy analysis.

IV. ANALYSIS

A. Assignment of resonant multiphoton detachment spectra of C_6^- and C_8^-

1. C_6^- spectrum

The band origin in the C_6^- multiphoton detachment spectrum in Fig. 2 occurs at 16 476 cm^{-1} (2.07 eV). This is very close to the band origin at 16 458 cm^{-1} seen by Maier[1] in absorption in a Ne matrix, confirming their assignment of

this band to C_6^-. Schmatz and Botschwina[10] calculate the term energy of the $C \, ^2\Pi_g$ electronic state of C_6^- to be 2.12 eV. Based on this comparison, we assign the features in our spectrum to the $C \, ^2\Pi_g \leftarrow X \, ^2\Pi_u$ electronic transition of C_6^-, in agreement with Maier's assignment. The main progression in our spectrum with a peak spacing of ca. 600 cm^{-1} was also seen in the matrix spectrum. In the same *ab initio* calculation by Schmatz and Botschwina, the harmonic vibrational frequency of the ν_3 mode of the $C \, ^2\Pi_g$ state was found to be 599 cm^{-1}, and we assign the main progression in our spectrum to this mode.

The peak at 18 294 cm^{-1} is most likely the 3_0^3 transition, as it lies 1818 cm^{-1} to the blue of the origin, and the nearby peak at 18 243 cm^{-1}, 1767 cm^{-1} from the origin, is assigned to the 2_0^1 transition; the calculated frequency for the ν_2 mode in the $C \, ^2\Pi_g$ state is 1805 cm^{-1}.[10] Given the closeness of these two peaks, there may be a Fermi resonance interaction between them that mixes their vibrational character. Based on the harmonic *ab initio* frequency, 2189 cm^{-1}, for the ν_1 mode, the cluster of peaks centered at 18 528 cm^{-1} (2070 cm^{-1} from the origin) is assigned to the 1_0^1 transition. These assignments and frequencies are in reasonable agreement with the matrix work.

Several peaks appear in our spectrum that were either very weak or not observed in the matrix spectrum. For example, the peaks at 16 696 and 16 965 cm^{-1} lie only 220 and 489 cm^{-1}, respectively, to the blue of the origin; these were not seen at all in the matrix spectrum. They mostly likely

represent double quanta excitation in low-frequency bending modes in the $C\ ^2\Pi_g$ state. The vibrational frequencies of the $X\ ^2\Pi_u$ state have been calculated using GAUSSIAN 92 at the UHF/6-31G* level and are reported in Table V; see Sec. IV C for more details. Assuming the vibrational frequencies of the $C\ ^2\Pi_g$ state are similar to those for the $X\ ^2\Pi_u$ state, the two peaks are assigned to the 9_0^2 and 8_0^2 transitions. The complete vibrational assignments of the C_6^- spectrum are listed in Table I; these include hot band transitions that yield vibrational frequencies in the anion ground state and combination bands not discussed above.

The additional peaks observed in our spectrum compared to the matrix study[1] are primarily due to saturation effects in the one-color multiphoton detachment experiment. In order to achieve sufficient detachment, the laser fluence used in these experiments is so high that it saturates the first excitation process, i.e., the $C\ ^2\Pi_g \leftarrow X\ ^2\Pi_u$ electronic transition, which is a strongly allowed optical transition. This distorts the intensity distribution, and nominally very weak transitions such as those involving bending excitation appear to be much stronger than in the weak-field limit; similar effects were seen in C_4^-.[13] In two-color multiphoton detachment, on the other hand, the excitation laser fluence can be greatly reduced, reducing saturation of the bound–bound transition. The effect of this is clear in Fig. 3, in which the relative intensity of the 8_0^2 transition at 16 965 cm^{-1} compared to the 3_0^1 transition is markedly less in the two-color spectrum than in the one-color spectrum. The peak narrowing in the two-color spectrum provides further evidence of saturation in the one-color spectrum.

2. C_8^- spectrum

The apparent origin of an electronic transition at 12 963 cm^{-1} in the C_8^- spectrum shown in Fig. 1 lies close to the calculated term energy,[11] 13 634 cm^{-1} of the $C\ ^2\Pi_u$ state of C_8^-, so we assign the first few peaks at the red end of our spectrum to the $C\ ^2\Pi_u \leftarrow X\ ^2\Pi_g$ transition. The corresponding band origin in the matrix spectrum[2] occurs at 12 933 cm^{-1}, slightly to the red as was also the case for C_6^-. The three peaks to the blue of the origin at 13 416, 13 920, and 15 050 cm^{-1} were also seen in the matrix spectrum; these features are more intense and broader in our spectrum, presumably due to saturation of the bound–bound transition. We assign these peaks based on the calculated vibrational frequencies and intensities by Schmatz and Botschwina.[11] The peak positions and assignments are given in Table II.

To the blue of these features, we observe several more peaks that were not reported in the matrix work. Several of these peaks are as intense as the $C \leftarrow X$ origin, and probably represent transitions to one or more higher-lying electronic states of C_8^-. The peak at 16 305 cm^{-1} is likely to be the origin of one these transitions, but we cannot make more definitive assignments in this region.

B. Resonant multiphoton detachment mechanism

In this section, we propose and discuss mechanisms for multiphoton detachment of C_4^-, C_6^-, and C_8^- that are in qualitative accord with our observations. A more quantitative analysis is presented in Sec. IV C.

1. C_4^-

No delayed emission is observed at any excitation energy for C_4^-. However, the comparison of the single- and multi-photon photoelectron spectra in Fig. 8 shows that the detachment mechanisms in the two experiments are very different. The structureless, monotonically decreasing (for eKE >0.1 eV) electron kinetic energy spectrum resulting from multiphoton excitation resembles the expected result for bulk thermionic emission, for which the kinetic energy distribution should be proportional to $\exp(-E/kT)$.[14] The one-photon photoelectron spectrum of W_n^- clusters shows a similarly monotonically decreasing eKE signal underlying structured features due to direct detachment.[31] This was interpreted as arising from the competition between two pathways subsequent to absorption of a single photon: direct detachment vs internal conversion followed by thermionic emission.

The lower C_4^- photoelectron spectrum in Fig. 8 was taken at $h\nu=2.71$ eV, at the energy of the $C\ ^2\Pi_u \leftarrow X\ ^2\Pi_g$ origin. Two photons are required for ejection of an electron; the electron affinity of C_4 is 3.88 eV.[4] This spectrum shows no evidence for direct detachment, and we propose the mechanism shown in Fig. 10 for the resonant two-photon detachment of C_4^-. This mechanism is comprised of the following sequence of events which lead to detachment of the negative ion: (1) absorption of the first photon, (2) internal conversion back to the ground electronic state, (3) absorption of the second photon, (4) internal conversion back to the ground electronic state and energy randomization, and (5) thermionic emission from the highly vibrationally excited anion ground state. In this mechanism, each photon absorption corresponds to an electronic transition from the $X\ ^2\Pi_g$ state to the $C\ ^2\Pi_u$ state, but the second absorption corresponds to a transition between two highly excited vibrational levels of the two electronic states. Similar mechanisms have been proposed to explain delayed electron emission after multiphoton excitation of neutral metal clusters.[16–18]

The absence of direct detachment in our spectrum is of interest. After absorbing the first photon at 2.71 eV, the anion is in the ground vibrational state of the $C\ ^2\Pi_u$ state. The second photon has sufficient energy to directly detach this state to the $C_4 + e^-$ continuum. However, the transition from the $C\ ^2\Pi_u$ state of C_4^- (molecular orbital configuration $\cdots 1\pi_u^3 1\pi_g^4$) to the linear ground state of neutral C_4 ($X\ ^3\Sigma_g^-$, $\cdots 1\pi_u^4 1\pi_g^2$) is not a one-electron transition and should have a very small cross section. A second photon can be absorbed more readily once internal conversion to the ground state has occurred.

Hence, regardless of the internal conversion rate after the first photon is absorbed, one would not expect *direct* two-photon detachment through the $C\ ^2\Pi_u$ state to be a facile process. For the mechanism in Fig. 10 to be operative, the
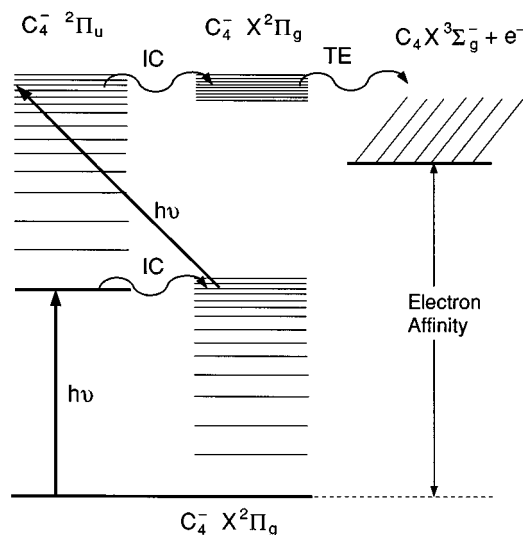
FIG. 10. Schematic drawing of C_4^- resonant two-photon detachment mechanism. IC stands for internal conversion, TE for thermionic emission.

only constraint on the rate of the first internal conversion step is that it occurs within 30 ns, the width of the laser pulse, so that the second photon can also excite the $C\ ^2\Pi_u \leftarrow X\ ^2\Pi_g$ transition. In addition, the thermionic emission rate must be sufficiently fast so that no delayed electron emission is observed. This point is considered further in Sec. IV C.

2. C_6^-

The multiphoton photoelectron spectrum of C_6^- at $h\nu$ =2.04 eV in the lower half of Fig. 9 resembles that of C_4^-. However, the electron affinity of linear C_6 is 4.18±0.01 eV,[4] so the absorption of two photons is insufficient to detach C_6^- to form linear C_6. Thus the spectrum in Fig. 9 results either from the absorption of at least three photons, or from the absorption of two photons followed by thermionic emission to a lower energy form of C_6. The latter possibility is quite intriguing, since many calculations have predicted the existence of a cyclic form of neutral C_6 that lies below the linear C_6 isomer.[37,38] Experimentally, only the linear isomer has been definitively identified. It is therefore crucial to determine the number of photons being absorbed in our experiments.

We first consider the one-color electron emission results in Figs. 4 and 6. From the power dependence studies alone, one would conclude that delayed electron emission, which is linear with laser fluence, results from absorption of a single photon, whereas prompt electron emission results from absorption of two photons. We observe delayed emission at photon energies as low as 2.37 eV (19 128 cm^{-1}). This implies that one-photon detachment occurs at photon energies as low as 1.81 eV below the electron affinity of linear C_6, and that the lower energy (presumably cyclic) isomer of C_6 is more stable than the linear isomer by at least 1.81 eV. Such a large separation is suspicious in light of the various calculations. For example, Raghavachari *et al.*[37] calculated

that the cyclic structure lies only 0.4 eV below the linear structure, and several other investigations[38] have yielded similar or smaller splittings.

One therefore has to reexamine the laser power dependence results. If the first step in the excitation process, the strongly allowed $C\ ^2\Pi_g \leftarrow X\ ^2\Pi_u$ transition, is saturated, then the power dependence may be misleading with respect to the number of photons absorbed. The spectra in Fig. 3 and those obtained in our study on C_4^- show that saturation of the bound–bound transition in a one-color experiment does occur.[13] The two-color experiments in Fig. 7 were performed in order to investigate more closely how many photons are responsible for the delayed and prompt electron emission.

The solid trace in the upper spectrum of Fig. 7 shows the electron emission as a function of time for two laser pulses separated in time by 200 ns, and the dotted trace in the same spectrum shows the result when the first laser is blocked. The photon energies are $h\nu_1$=2.12 eV (17 077 cm^{-1}) and $h\nu_2$=2.84 eV (22 873 cm^{-1}). A comparison of the two traces shows that delayed electron emission occurs only when the ions are irradiated with both lasers. Hence, at least two photons are required for delayed emission to occur, not just one as implied by the power dependence. In the bottom spectrum of Fig. 7, the electron emission profiles are compared for the two-color experiment (solid trace) and a one-color experiment (dotted energy) at photon energy $h\nu_3$=2.48 eV, where $2h\nu_3 = h\nu_1 + h\nu_2$. The time constants for the decay of the electron emission are the same for the two curves. This implies that (a) the delayed emission in both experiments results from absorption of two photons, and (b) the rate of delayed emission depends only on the total energy absorbed by the ion, not on the specifics of the excitation process.

The second result is exactly what one would expect for an activated statistical process in which complete energy randomization occurs prior to electron emission, supporting the idea that the delayed electron emission can be thought of as thermionic emission from a highly vibrationally excited anion. The first result means that we no longer need to invoke the existence of a low-lying cyclic state of C_6 to explain the presence of delayed emission; if this is a two-photon process, then formation of linear C_6 is energetically possible at all photon energies in Fig. 4 where delayed emission occurs.

We can now explain all of the detachment results for C_6^-. The power dependence studies show that at excitation energies where both delayed and prompt electron emission are observed, the prompt electron emission has a higher order dependence on laser fluence. The above discussion thus indicates that at these energies, prompt emission is from a three-photon process. The explanation for the trends in Fig. 4 is then as follows. At the lowest photon energies, delayed emission from two-photon absorption is too slow to observe in our time window of several hundred nanoseconds, so all that remains is the prompt emission from three-photon absorption. Towards higher photon energies, the emission rate from two-photon absorption becomes sufficiently rapid that it cannot be distinguished from emission following three-photon absorption.
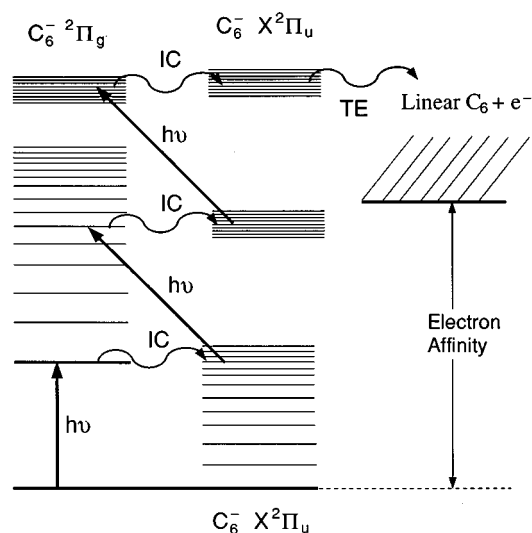
FIG. 11. Schematic drawing of C_6^- resonant multiphoton detachment mechanism for excitation at the band origin of the $C\,^2\Pi_g \leftarrow X\,^2\Pi_u$ transition. IC stands for internal conversion, TE for thermionic emission.
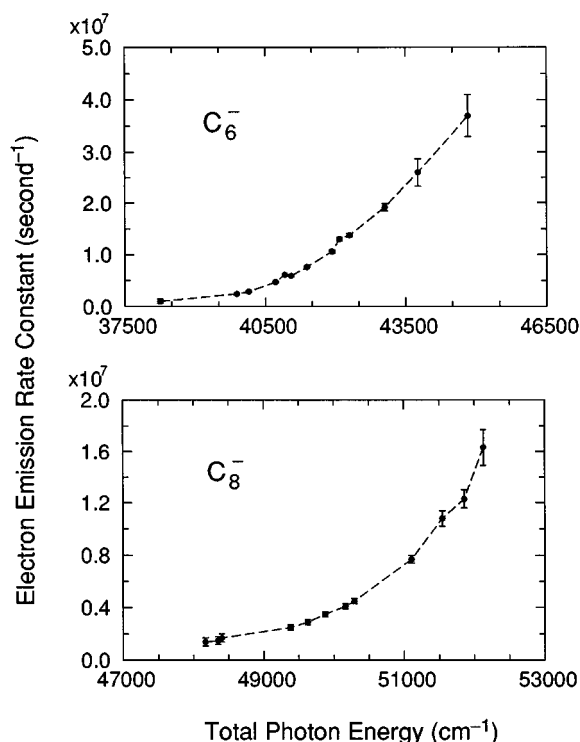

FIG. 12. Measured electron emission rate constants at various total photon energies. Dashed lines are drawn as a visual guide. The error bars in the measurement are as indicated in the figure; for some data points, error bars are smaller than the size of solid circles that are used to represent the data points.

Thus, the multiphoton photoelectron spectrum of C_6^- in Fig. 9 is due to the absorption of three photons. The total photon energy absorbed is 6.12 eV, which is 1.94 eV above the EA of linear C_6. The proposed mechanism for electron detachment at this energy is shown in Fig. 11. It is similar to that proposed for C_4^-, with one additional photon absorption and internal conversion step required prior to emission of an electron from a highly vibrationally excited level of the anion ground electronic state.

3. C_8^-

The concepts used to explain the C_6^- results can be extended to explain the more complicated electron emission results for C_8^- in Fig. 5. In contrast to the results for C_6^-, delayed emission is observed at the origin of the $C\,^2\Pi_u \leftarrow X\,^2\Pi_g$ band at 12 963 cm^{-1}. As the photon energy is increased, the delayed emission first becomes indistinguishable from the prompt emission, but it becomes apparent again as the photon energy is further increased. The key to understanding this trend is the identical rates for delayed emission observed at $h\nu_1 = 12\,963$ cm^{-1} and $h\nu_2 = 17\,286$ cm^{-1}. We note that $4h\nu_1 = 3h\nu_2$. Since, as implied by the C_6^- results, the emission rate depends only on the total energy absorbed, the equal rates at the two energies imply that the delayed emission at $h\nu_1$ is due to the absorption of four photons, whereas that at $h\nu_2$ is due to the absorption of three (higher energy) photons.

The electron affinity of linear C_8 is 4.38 eV (35 320 cm^{-1}), so only three photons are needed to detach C_8^- at the origin to form linear C_8. Based on the above considerations, it would appear that the emission rate after three photon absorption is sufficiently slow that absorption of a fourth photon during the laser pulse is a more likely event. In any case, we do not need to invoke a lower energy cyclic C_8 isomer to explain our results.

C. Analysis using microcanonical rate theory

The considerations discussed above have enabled us to determine the number of absorbed photons responsible for the delayed electron emission from C_6^- and C_8^-. The results are given in Table III and Table IV. Figure 12 shows the rate constant as a function of total absorbed photon energy for C_6^- and C_8^-.

One can now more quantitatively model both the electron kinetic energy distributions and electron emission rates resulting from multiphoton absorption. In the previous section, we showed that both of these were qualitatively what one would expect from thermionic emission from a cluster. In this section, the experimental results are compared to the predictions of a statistical model for thermionic emission from clusters developed by Klots.[15] Our approach differs from previous comparisons of this type in that the internal energy rather than the temperature of our clusters is assumed to be well defined. This is reasonable, given that our clusters are initially cold and then absorb a known amount of energy from the laser field. We therefore use the microcanonical version of Klots's model; a similar microcanonical treatment has been discussed by Schlag and Levine.[39]

In this model, the rate of electron emission $k(E)$ is given by

$$k(E) = \frac{W(E, E_0)}{h\rho(E)}. \tag{1}$$

TABLE V. Vibrational frequencies (in cm^{-1}) used in microcanonical rate constant calculations.

$C_4^-(X\,^2\Pi_g)$	$C_4(X\,^3\Sigma_g^-)$	$C_6^-(X\,^2\Pi_u)$	$C_6(X\,^3\Sigma_g^-)$	$C_8^-(X\,^2\Pi_g)$	$C_8(X\,^3\Sigma_g^-)$
π_u 240	π_u 188	π_u 119	π_u 105	π_u 60	π_u 60
π_g 505	π_g 367	π_g 261	π_g 238	π_g 68	π_g 203
σ_g 893	σ_g 919	π_u 437	π_u 331	π_u 265	π_u 153
σ_u 1884	σ_u 1566	π_g 540	π_g 496	π_g 284	π_g 320
σg 2084	σ_g 2111	σ_g 628	σ_g 649	π_u 546	π_u 264
		σ_u 1167	σ_u 1194	π_g 515	π_g 501
		σ_g 1823	σ_g 1661	σ_g 481	σ_g 497
		σ_u 1943	σ_u 1971	σ_u 918	σ_u 944
		σ_g 2171	σ_g 2176	σ_g 1303	σ_g 1346
				σ_u 1783	σ_u 1680
				σ_g 1915	σ_g 1945
				σ_u 2083	σ_u 2097
				σ_g 2151	σ_g 2154

Here, E is the total energy, E_0 is the threshold for electron ejection (i.e., the electron affinity), $\rho(E)$ is the vibrational density of anion states, and $W(E,E_0)$ is the total number of energetically accessible product states, taking into account the orbital angular momentum of the departing electron. This last term is given by

$$W(E,E_0) = \int_0^{E-E_0} dx\; \rho_\nu(x) \left\{ 1 + 2\left[\frac{2\mu b^2(E-E_0-x)}{\hbar^2}\right]^{1/2} \right.$$
$$\left. + \left[\frac{2\mu b^2(E-E_0-x)}{\hbar^2}\right] \right\}, \tag{2}$$

where μ is the reduced (i.e., electron) mass, b is the classical hard-sphere collision radius, and ρ_ν is the density of vibrational states of the neutral species. One must also include a spin-degeneracy factor for the outgoing electron and an electronic degeneracy factor for anion and neutral.

In deriving Eq. (2), the following expression for the electron kinetic energy distribution $p(\epsilon)$ was used

$$p(\epsilon) = \rho_\nu(E-E_0-\epsilon)(L_{max}+1)^2, \tag{3}$$

where

$$L_{max}+1 = (\lambda+b)/\lambda \tag{4}$$

and λ is the de Broglie wavelength of the ejected electron. Equations (1) and (3) can be directly compared to our experimental results, provided that we can calculate the density of vibrational levels, ρ and ρ_ν, in the anion and neutral. To do this, the vibrational frequencies of the neutral and anion ground state are obtained through *ab initio* calculations using GAUSSIAN 92 at the UHF/6-31G* level. For the neutral species, our calculated frequencies are identical to those reported by Martin *et al.*[40] at the same level of calculation. For C_8^-, one of the bending frequencies (the ν_{13} mode) came out negative; this is discarded. Instead, the frequency of the same mode of neutral C_8 is substituted. One of the π_g bending frequencies (the ν_{10} mode) of C_8 is found to be imaginary at UHF/6-31G* level. This frequency is discarded and the frequency of the same mode obtained in an *ad hoc* MNDO calculation is used.[40] The UHF frequencies are scaled by 90%. The vibrational frequencies after scaling are shown in

Table V. The Whitten–Rabinovitch approximation[41] is then used to calculate the vibrational density of states. Each stretching mode is considered as a one-dimensional harmonic oscillator, and each doubly degenerate bending mode is treated as two one-dimensional harmonic oscillators with the same frequency.

Electron affinity values are known from previous work. The value of b, the classical hard-sphere collision radius is taken to be one half of the total carbon chain length. The spin multiplicity is equal to 2, the neutral electronic multiplicity (of the $^3\Sigma_g^-$ state) is 3, and the anion electronic multiplicity (of the $^2\Pi$ state) is 4. If nuclear spin statistics is taken into account, both the number of neutral states and the density of anion states should be divided by a factor of 2, so the rate given by Eq. (1) is unchanged.

When comparing the calculated rate constant to the experimental value, one should include the thermal energy in the cluster anion prior to photon excitation. The thermal energy is estimated as

$$E_{thermal} = (3N-5)k_B T_{vib}. \tag{5}$$

The vibrational temperature of the negative ions in our source, T_{vib}, is estimated to be 100 K from the observed hot band transition intensities in the C_6^- multiphoton detachment spectrum (see Fig. 1). At this temperature, adding $E_{thermal}$ to the energy from photon absorption approximately doubles the calculated rate constant in the photon energy region of interest.

The rate constants for the photon energy region for which delayed emission was observed are calculated using the parameters described above, including $E_{thermal}$. The results are displayed and compared with the experimental rates in Fig. 13. The calculated rate constants follow the same trends as the experimental rate constants but are high by a factor of 10 for C_6^- and a factor of 2–3 for C_8^-. Calculations on C_4^- were also performed assuming two-photon absorption. These predicted prompt electron emission over the entire energy range we studied, consistent with our observations. Overall, agreement is quite good considering no adjustable parameters are used in the calculations.

In Fig. 14, the experimental multiphoton photoelectron spectra of C_4^- and C_6^- are compared to spectra calculated from Eq. (3). In the calculation, we assumed *s*-wave emission only, so that $L_{max}=0$ for all electron kinetic energies. One can easily allow L_{max} to vary with energy according to Eq. (4), but this results in somewhat poorer agreement with experiment. In any case, while the overall shape of the experimental and calculated spectra agree, the experimental distribution clearly has more intensity at low electron kinetic energy than the calculated distribution.

In principle, one should include the lower-lying A and B doublet states predicted for all three anions[9–11] when calculating the anion density of states, since the available energy should be randomized among electronic as well as vibrational degrees of freedom. The inclusion of these states will increase $\rho(E)$ in Eq. (1), therefore decreasing the calculated emission rate and improving the agreement with experiment. In fact, the inclusion of these states at their calculated term
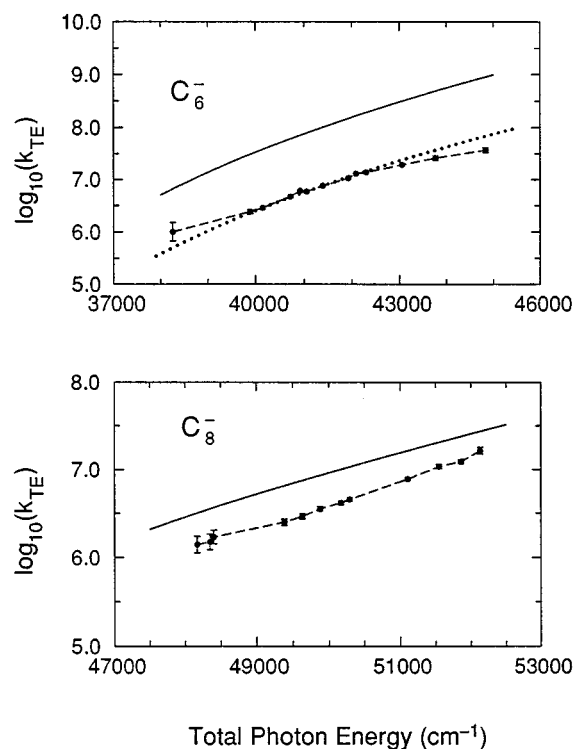
FIG. 13. Comparison of calculated and experimental electron emission rate constants. Rates are calculated from Eq. (1) in the text: For C_6^-, two calculations (dotted line and solid line) differing in values used for anion vibrational frequencies are shown (see the text). For C_8^-, only one calculation is shown (solid line); Experimental results are shown in solid circles connected by a dashed line.

FIG. 14. Calculated photoelectron spectra of C_4^- and C_6^- (dashed lines) using Eq. (3) and assuming *s*-wave detachment, compared to experimental multiphoton photoelectron spectra from Figs. 8 and 9 (solid lines). The total energies used in the calculations correspond to two-photon absorption ($2h\nu$ =5.42 eV) for C_4^- and three-photon absorption ($3h\nu$=6.12 eV) for C_6^-.

energies has an insignificant effect on the calculated rate constants, because the contribution to $\rho(E)$ from the ground state is so dominant.

One must consider the sensitivity of the calculations to the values assumed for the anion and neutral vibrational modes. The lowest frequency modes have the largest effect on the density of states. By lowering the lowest vibrational frequency (ν_9) of C_6^- from 119 cm^{-1} (the value in Table V) to 37 cm^{-1}, the calculated rate constant at photon energy 41 390 cm^{-1} matches the experimentally measured value, and agreement is excellent across the full energy range probed in our experiment; see the dotted line in Fig. 13. This is an unrealistically low frequency for the ν_9 mode. One can also obtain good agreement with the experimental emission rates by decreasing the four lowest anion frequencies by 30%. However, neither of these adjustments affect the neutral $\rho_v(E)$ and therefore do not improve the agreement between the calculated and experimental photoelectron spectrum in Fig. 14. If the lowest neutral frequencies are made smaller, the calculated photoelectron spectrum shifts towards lower electron kinetic energy, but then the calculated emission rate increases. It therefore appears that the discrepancies between experiment and the statistical predictions cannot be remedied by small adjustments of the vibrational frequencies.

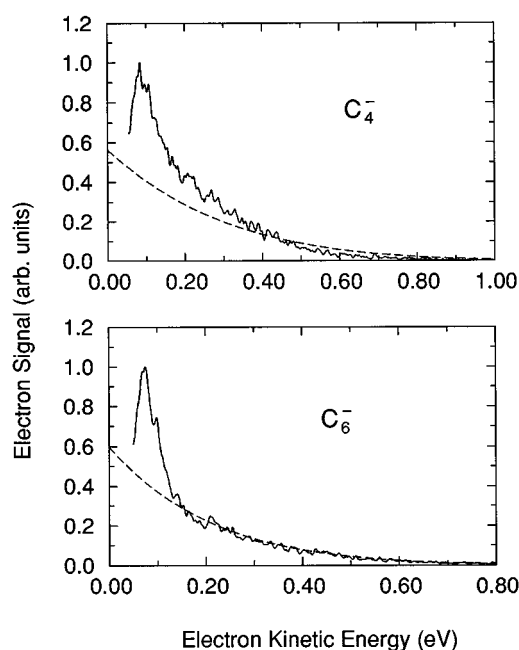A more likely cause of at least some of the differences between the experimental and calculated results in Figs. 13 and 14 is the neglect of anharmonicity in our calculation of the vibrational densities of states. This means that the vibrational densities of states in both the anion and neutral are increasingly underestimated as the internal energy is raised. As a result, the calculated rate constants would be lower, since the internal energy of the anion is greater than that of the neutral by E_0, the electron affinity. Moreover, the calculated electron energy distribution would shift towards lower eKE.

Overall, the agreement between experimental and calculated results is quite reasonable and might be improved with a more sophisticated calculation of the densities of states. It therefore appears justified to claim that we are observing the analog of thermionic emission from these very small clusters. This is considered further in the following section.

V. DISCUSSION

A. Mechanism for electron emission

The above analysis supports the overall mechanism for resonant multiphoton detachment shown in Figs. 10 and 11. The main features of this mechanism are (1) fast internal conversion to the ground electronic state following absorption of each photon, and (2) thermionic emission from the highly excited ground state once enough photons have been absorbed. It is quite striking that such a mechanism would apply to species as small as the carbon cluster anions considered here. In this section several features of this mechanism are considered in more detail.

Much of the discussion so far has focused on the dynamics of the electron emission process. However, the multiple photon absorption/internal conversion steps are also of interest. As mentioned in Sec. IV B 1, once the first photon is absorbed, internal conversion must take place within the time that the laser pulse is on, ~30 ns, so that more photons can be absorbed. Thus the minimum internal conversion rate is 3.3×10^7 s^{-1}. The internal conversion rate is presumably driven by the high vibrational level density of the ground electronic state; at the band origin of the $C \leftarrow X$ transition in the three anions, the level densities are 6.6×10^3, 7.4×10^7, and 6.0×10^{11} per cm^{-1} for C_4^-, C_6^-, and C_8^-, respectively.

An upper bound to the internal conversion rate can be obtained from the peak widths in the multiphoton detachment spectra. In the two-color resonant two-photon detachment spectrum of C_4^-,[13] rotational features were observed and the peaks were about 0.1 cm^{-1} wide, indicating that internal conversion rate is less than 10^{10} s^{-1}. The upper and lower bounds to the internal conversion rate along with the above density of states can be used in Fermi's golden rule to estimate the average coupling matrix element between the C and X states of C_4^-; this lies between 6.5×10^{-5} and 1.1×10^{-3} cm^{-1}. The lower bound is probably more meaningful because a significant fraction of the peak widths is from the lasers used in the experiment. The broader peaks in the C_6^- and C_8^- spectra arise at least in part from a combination of saturation and unresolved rotational structure, so it is less useful to extract information on the internal conversion rate from them.

Our results show that one or more photons in excess of what is needed energetically to eject an electron may be required in order to observe electron emission on the time scale of our experiment; at the origin of the $C \leftarrow X$ band of C_8^-, for example, the delayed emission shown in Fig. 5 results from the absorption of four photons, even though only three are required energetically. This is a clear example of a ''kinetic shift,'' defined as the amount of energy above the electron affinity required to give rise to a thermionic emission rate observable in the experiment (faster than ca. 5×10^5 per s). Experimentally, we find the kinetic shifts for C_6^- and C_8^- to be around 0.50 and 1.4 eV, respectively, and the kinetic shift for C_4^- is calculated to be around 0.25 eV.

Our proposed mechanism does not consider dissociation of the highly excited clusters as an alternative to electron emission. This is because in negative ions in general, and carbon cluster anions in particular, electron detachment is a lower energy channel than fragmentation. For example, the binding energy of C_6^- relative to the lowest energy channel $C_3 + C_3^-$ is calculated to be approximately 5.5 eV,[42] whereas the detachment threshold is only 4.18 eV. Thus while fragmentation can certainly be incorporated into our analysis, it is likely to be a minor channel relative to detachment. This is supported by a previous study in which the quantum yield for dissociation of carbon cluster anions subsequent to multiphoton absorption was found to be considerably less than unity.[43] A more detailed consideration of the competition between ionization and dissociation in clusters is given by Schlag and Levine.[39]

As mentioned in Sec. I, thermionic emission has been observed from larger and more complex clusters than the small carbon cluster anions studied here, and a similar mechanism to ours has been proposed to explain thermionic emission from metal clusters following multiphoton excitation. The most detailed work along these lines has been performed by Collings *et al.*[18] on Nb clusters, in which the delayed ionization rate was measured as both the internal temperature and laser excitation energy of the clusters were varied. The rates were fit very well by an Arrhenius-type expression, but the preexponential A factor was found to be about a factor of 100 less than expected. This is reminiscent of our results, in which the microcanonical model correctly reproduces the dependence of the emission rate on internal energy but systematically overpredicts the rate.

This discrepancy raises the issue of the validity of the two assumptions behind the statistical model, namely that (a) energy is rapidly randomized between vibrational and electronic degrees of freedom, and (b) all accessible product states are formed with unit probability. The energy randomization hypothesis assumes the free and rapid flow of energy between vibrational to electronic motion, ultimately resulting in electron detachment. However, if vibrational to electronic energy transfer were the rate-determining step, one would observe a slower emission rate than that calculated by Eq. (1). Regarding the second assumption, Klots[15] points out that for emission from negative ions, the Wigner threshold law[44] reduces the probability for formation of product states corresponding to low electron kinetic energies, because the photodetachment cross section does not rise infinitely sharply at the detachment threshold. This would lower the overall calculated emission rate, but would not improve agreement with the experimental electron kinetic energy distributions (see Fig. 14). Moreover, the Wigner threshold law does not affect the cross section near threshold for ionization from neutrals, so this cannot be the reason for the discrepancy seen by Collings *et al.*[18]

While it is intriguing to consider these possible defects in the statistical picture of thermionic emission from clusters, one should realize that the experimental and statistical rates for C_6^- and C_8^- are within an order of magnitude. Also, as mentioned in the previous section, the inclusion of anharmonicity in the reactant and product density of states (or calculation of the A factor) would reduce the calculated emission rates and shift the calculated electron kinetic energy distribution in the right direction. Thus, deviations from the statistical model appear to be at most rather minor, at least for the anions studied here.

B. Implications for other photodetachment studies of carbon cluster anions

Zajfman *et al.* have reported electron photodetachment cross sections of small carbon cluster anions.[45] In their experiments, carbon cluster anions produced by either ion sputtering or pulsed beam/laser vaporization were photodetached by various pulsed lasers. The photodetachment cross section was measured both as a function of laser photon energy and

as a function of laser power at fixed photon energy. When generated in the sputtering source, the C_4^-, C_6^-, and C_8^- anions were found to have significantly lower electron detachment thresholds than expected based on the electron affinity of the linear carbon clusters. For example, C_8^- was found to photodetach at a photon energy as low as 1.16 eV. Furthermore, they concluded the photodetachment process was a single-photon event based on laser power dependence studies which showed a linear dependence at lower laser power and saturation at higher laser power. These observations were taken as evidence for the existence of cyclic forms of the three anions, since the cyclic neutral isomers are predicted to have considerably lower electron affinities than the linear isomers.

Our results suggest that Zajfman *et al.* may have been observing multiphoton detachment of hot linear anions, rather than one-photon detachment of cyclic anions. We observe efficient resonant multiphoton detachment for all three linear anions in the same energy range as the thresholds seen by Zajfman *et al.* For example, they assign the detachment threshold of C_4^- to be 2.1 eV, whereas the origin of the $C \leftarrow X$ transition in C_4^- occurs at 2.71 eV; the lower threshold in their experiment could well be due to the high temperature of the ions produced in their sputtering source. Moreover, the analysis in Sec. IV B shows that power dependences are misleading in the presence of a strongly allowed transition; recall that the delayed electron emission from C_6^- exhibited a linear power dependence (Fig. 6) but was shown in the two-color experiments (Fig. 7) to arise from two-photon absorption. Hence, a combination of multiphoton detachment and laser saturation effects may have led to a misleading interpretation of the earlier experiments.

VI. CONCLUSIONS

The electronic spectroscopy of C_4^-, C_6^-, and C_8^- was studied using resonant multiphoton detachment, and the electron detachment dynamics of these anions subsequent to multiphoton absorption were investigated by measurements of the photoelectron spectrum and electron emission rate. The resonant multiphoton spectra yield vibrationally resolved bands corresponding to the $C\ ^2\Pi \leftarrow X\ ^2\Pi$ electronic transitions in each anion. The band origins and vibrational frequencies for transitions near the origins are in good agreement with previous matrix spectra and *ab initio* calculations, showing that we are observing transitions between two linear electronic states of the anions. However, the C_8^- spectra in particular is quite complex and likely contains more than one electronic transition.

The photoelectron spectra and electron emission rates following multiphoton absorption provide compelling evidence for electron ejection via the cluster analog of thermionic emission. This interpretation is supported by comparing both sets of results with a microcanonical statistical treatment developed to model thermionic emission from clusters. Thermionic emission from fullerenes and small metal clusters has been observed previously, but the carbon cluster anions studied here represent the smallest systems to date

that exhibit this phenomenon. Since electron detachment energies are generally lower than bond dissociation energies in negative ions, the mechanism for thermionic emission discussed here is likely to apply to multiphoton excitation of other negative ions.

Finally, our results have some bearing on the controversy concerning the relative stability of linear vs cyclic carbon clusters. Our initial interpretation of the C_6^- photoelectron spectra and electron emission rates suggested that detachment to an isomer of C_6 lying lower in energy than linear isomer was occurring; this presumably would be the cyclic isomer. However, a more careful investigation showed that it is not necessary to invoke a low energy isomer, and that all of our results for the three anions are consistent with photodetachment to linear neutral carbon clusters. Moreover, our results suggest that earlier experiments on carbon cluster anions in which low detachment thresholds were attributed to cyclic anions may have been misinterpreted, and that the low thresholds may well have resulted from multiphoton absorption of the linear anions.

[1] D. Forney, J. Fulara, P. Freivogel, M. Jakobi, D. Lessen, and J. P. Maier, J. Chem. Phys. **103**, 43 (1995).

[2] P. Freivogel, J. Fulara, M. Jakobi, D. Forney, and J. P. Maier, J. Chem. Phys. **103**, 54 (1995).

[3] S. Yang, K. J. Taylor, M. J. Craycraft, J. Conceicao, C. L. Pettiette, O. Cheshnovsky, and R. E. Smalley, Chem. Phys. Lett. **144**, 431 (1988).

[4] D. W. Arnold, S. E. Bradforth, T. N. Kitsopoulos, and D. M. Neumark, J. Chem. Phys. **95**, 8753 (1991).

[5] H. Handschuh, G. Gantefor, B. Kessler, P. S. Bechthold, and W. Eberhardt, Phys. Rev. Lett. **77**, 1095 (1995).

[6] T. N. Kitsopoulos, C. J. Chick, Y. Zhao, and D. M. Neumark, J. Chem. Phys. **95**, 5479 (1991).

[7] C. C. Arnold, Y. Zhao, T. N. Kitsopoulos, and D. M. Neumark, J. Chem. Phys. **97**, 6121 (1992).

[8] G. V. Helden, P. R. Kemper, N. G. Gotts, and M. T. Bowers, Science **259**, 1300 (1993).

[9] S. Schmatz and P. Botschwina, Int. J. Mass. Spectrom. Ion Proc. **149**, 621 (1995).

[10] S. Schmatz and P. Botschwina, Chem. Phys. Lett. **235**, 5 (1995).

[11] S. Schmatz and P. Botschwina, Chem. Phys. Lett. **245**, 136 (1995).

[12] M. Ohara, H. Shiromaru, Y. Achiba, K. Aoki, H. Hashimoto, and S. Ikuta, J. Chem. Phys. **103**, 10393 (1995).

[13] Y. Zhao, E. de Beer, and D. M. Neumark, J. Chem. Phys. (in press).

[14] N. W. Ashcroft and N. D. Mermin, *Solid State Physics* (Holt, Rinehart, and Wilson, Philadelphia, 1976), pp. 362–364.

[15] C. Klots, Chem. Phys. Lett. **186**, 73 (1991).

[16] A. Amrein, R. Simpson, and P. Hackett, J. Chem. Phys. **94**, 4663 (1991); **95**, 1781 (1991).

[17] T. Leisner, K. Athanassenas, D. Kreisle, E. Recknagel, and O. Echt, J. Chem. Phys. **99**, 9670 (1993).

[18] B. A. Collings, A. H. Amrein, D. M. Rayner, and P. A. Hackett, J. Chem. Phys. **99**, 4174 (1993).

[19] E. E. B. Campbell, G. Ulmer, and I. V. Hertel, Phys. Rev. Lett. **67**, 1986 (1991).

[20] P. Wurz and K. R. Lykke, J. Chem. Phys. **95**, 7008 (1991).

[21] P. Sandler and C. Lifshitz, Chem. Phys. Lett. **200**, 445 (1992).

[22] K. W. Kennedy and O. Echt, J. Phys. Chem. **97**, 7088 (1993).

[23] D. Ding, R. N. Compton, R. E. Haufler, and C. E. Klots, J. Phys. Chem. **97**, 2500 (1993).

[24] Y. Zhang and M. Stuke, Phys. Rev. Lett. **70**, 3231 (1993).

[25] P. M. St. John, C. Yeretzian, and R. L. Whetten, J. Phys. Chem. **96**, 9100 (1992); C. Yeretzian, K. Hansen, and R. L. Whetten, Science **260**, 652 (1993).

[26] L. H. Andersen, C. Brink, H. K. Haugen, P. Hvelplund, D. H. Yu, N. Hertel, and S. P. Moller, Chem. Phys. Lett. **217**, 204 (1994).

[27] P. Demirev, G. Brinkmalm, J. Eriksson, R. Papaleo, P. Hakansson, and B. U. R. Sundqvist, Phys. Rev. B **50**, 9636 (1994).

[28] D. Ding, J. Huang, R. N. Compton, C. E. Klots, and R. E. Haufler, Phys. Rev. Lett. **73**, 1084 (1994).

[29] K. R. Lykke, Phys. Rev. Lett. **75**, 1234 (1995); M. Stuke and Y. Zhang, *ibid*. **75**, 1235 (1995).

[30] L.-S. Wang, J. Conceicao, C. Jin, and R. E. Smalley, Chem. Phys. Lett. **182**, 5 (1991).

[31] H. Weidele, D. Kreisle, and E. Recknagel, G. Schulze Icking-Konert, H. Handschuh, G. Ganteför, and W. Eberhardt, Chem. Phys. Lett. **237**, 425 (1995).

[32] T. N. Kitsopoulos, I. M. Waller, J. G. Loeser, and D. M. Neumark, Chem. Phys. Lett. **159**, 300 (1989).

[33] R. B. Metz, A. Weaver, S. E. Bradforth, T. N. Kitsopoulos, and D. M. Neumark, J. Chem. Phys. **94**, 1377 (1990).

[34] D. L. Osborn, D. J. Leahy, D. R. Cyr, and D. M. Neumark, J. Chem. Phys. **104**, 5026 (1996).

[35] J. M. Bakker, J. Phys. E **6**, 785 (1973); **7**, 364 (1974).

[36] C. Xu, G. R. Burton, T. Taylor, and D. M. Neumark (manuscript in preparation).

[37] K. Raghavachari, R. A. Whiteside, and J. A. Pople, J. Chem. Phys. **85**, 6623 (1986); K. Raghavachari and J. S. Binkley. *ibid*. **87**, 2191 (1987).

[38] J. Hutter, H. P. Luthi, and F. Diderich, J. Am. Chem. Soc. **116**, 750 (1994); V. Pless, H. U. Suter, and B. Engels, J. Chem. Phys. **101**, 4042 (1994); J. M. L. Martin and P. R. Taylor, J. Phys. Chem. **100**, 6047 (1996).

[39] E. W. Schlag and R. D. Levine, J. Phys. Chem. **96**, 10608 (1992).

[40] J. M. L. Martin, J. P. Francois, and R. Gijbels, J. Chem. Phys. **93**, 8850 (1990).

[41] G. Z. Whitten and B. S. Rabinovitch, J. Chem. Phys. **38**, 2466 (1963).

[42] J. D. Watts and R. J. Bartlett, J. Chem. Phys. **97**, 3445 (1992).

[43] M. J. DeLuca and M. A. Johnson, Chem. Phys. Lett. **152**, 67 (1988).

[44] E. P. Wigner, Phys. Rev. **73**, 1002 (1948).

[45] D. Zajfman, H. Feldman, O. Heber, D. Kella, D. Majer, Z. Vager, and R. Naaman, Science **258**, 1129 (1992).